A Theoretical Framework for Performance Characterization of Elastography: The Strain Filter

Tomy Varghese, *Member, IEEE*, and Jonathan Ophir

***Abstract*—This paper presents a theoretical framework for performance characterization in strain estimation, which includes the effect of signal decorrelation, quantization errors due to the finite temporal sampling rate, and electronic noise. An upper bound on the performance of the strain estimator in elastography is obtained from a strain filter constructed using these limits. The strain filter is a term used to describe the nonlinear filtering process in the *strain domain* (due to the ultrasound system and signal processing parameters) that allows the elastographic depiction of a limited range of strains from the compressed tissue. The strain filter predicts the elastogram quality by specifying the elastographic signal-to-noise ratio (SNR_e), sensitivity, and the strain dynamic range at a given resolution. The dynamic range is limited by decorrelation errors for large tissue strain values, and electronic noise for low strain values. Tradeoffs between different techniques used to enhance elastogram image quality may also be analyzed using the strain filter.**

I. Introduction

ULTRASONIC TECHNIQUES for measuring the elasticity of compliant tissue generally rely on the estimation of the strain [1]–[5]. Elastography, a technique of estimating the axial strain using differential displacements of the tissue elements due to tissue compression, was proposed by Ophir *et al.* [1].

This paper introduces the strain filter concept for the performance characterization of the strain estimator in elastography. The behavior of the upper bound of the SNR_e as a function of axial tissue strain forms a bandpass filter in the *strain domain*. The *strain domain* refers to the entire range of strains present in the compressed tissue. The strain filter consists of a graphical and analytical representation of the allowable range of strain values and their resulting SNR_e for a given elastographic resolution. The width of the strain filter specifies the dynamic range, and its height the respective SNR_e value of the estimated strain.

A block diagram elucidating the strain filter concept is presented in Fig. 1. Elastography uses small mechanical compressions on soft biological tissue that have a wide range of elastic moduli. A distribution of strains in the medium is caused by the quasi-static compression under certain mechanical boundary conditions. The input to the strain filter is the actual tissue strain characterized by an *infinite* dynamic range and SNR_e, fine (denoted by ϵ where epsilon is a very small number) resolution and sensitivity. However, the interaction of the actual tissue strain with the ultrasound system and signal processing parameters corrupts the elastogram obtained, in the sense that it now has a *finite* dynamic range, SNR_e, sensitivity, and resolution. The strain filter predicts the elastographic image quality (SNR_e, sensitivity, and dynamic range at a given resolution) in terms of the signal processing and system parameters used to obtain the elastogram. The strain filter therefore provides a quantitative assessment of the elastogram quality, in terms of the four parameters described above.

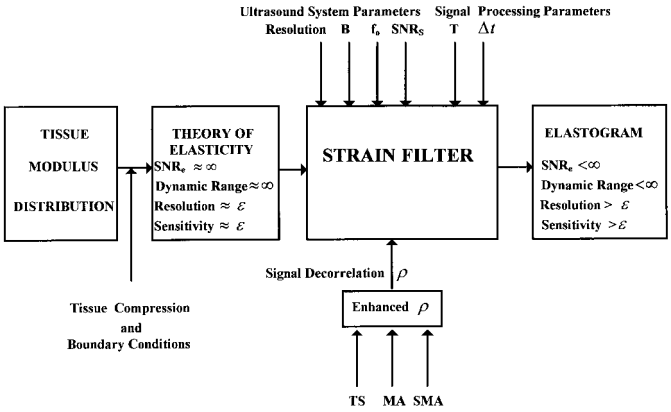

Fig. 1. The block diagram of the strain filter, indicating the filtering of the tissue strains by the strain filter to predict the dynamic range and respective SNR_e at a given resolution in the elastogram. The tissue strain measured using the ultrasound system is obtained by a quasi-static tissue compression restricted by the mechanical boundary conditions. The contributions of the signal processing and ultrasound system parameters are indicated as inputs into the strain filter. Improvements in estimator performance due to other techniques are explained by the enhancement in the correlation coefficient (reduced signal decorrelation).

In addition, the strain filter makes it possible to select the appropriate ultrasound system and signal processing parameters to obtain the best possible elastogram under given tissue conditions. In subsequent sections of this paper we discuss the effects of the various ultrasound system parameters such as pulse center frequency and band-

Manuscript received November 27, 1995; accepted July 15, 1996. This work was supported in part by NIH grants R01-CA38515, R01-CA60520, and P01-CA64579, and by a grant from Diasonics Corp., Santa Clara, CA.

T. Varghese and J. Ophir are with the Ultrasonics Laboratory, Department of Radiology, University of Texas Medical School, Houston, TX 77030 (e-mail: tomyv@msrad3.med.uth.tmc.edu).

width, and signal processing parameters (window size and overlap factor). Tradeoffs among different parameters and techniques that enhance elastogram quality may be evaluated and predicted using the strain filter. As illustrated in Fig. 1, techniques such as temporal stretching (TS) [6]–[8], multicompression averaging (MA) [5],[9],[10], and stretching multicompression averaging (SMA) [9],[10], reduce signal decorrelation, i.e. improve the correlation coefficient, thereby enhancing the performance of the strain filter. The improvements in the elastogram obtained using these techniques may be quantitatively predicted using the strain filter.

The ideal strain filter therefore has an infinitely high, flat all-pass characteristic shape in the strain domain, which means that all local tissue strains are displayed in the elastogram with infinite SNR_e; it also means that the strain dynamic range in the elastogram is infinite as well. Practical strain filters, however, have a bandpass characteristic shape in the strain domain, where the -3 dB width of this bandpass characteristic may be defined as the elastographic dynamic range. Under typical conditions, a -3 dB dynamic range of ≈ 30 dB is predicted by the strain filter; this is consistent with the range of strains measured experimentally using a single compression.

A description of the literature used to develop the strain filter is presented in Section II. The theoretical model for the strain filter is developed in Section III. Simulations to validate the theoretical model are presented in Section IV. The contributions of this paper are summarized in Section V.

II. Background

Development of the strain filter concept is based on obtaining the tightest bound on the variance of the strain estimator that includes all noise sources. Since the strain estimator uses time-delay (displacement) estimation to compute strain, the vast literature on time-delay estimation can be adapted for the strain estimation problem.

A. Noise Sources

The Cramér-Rao lower bound (CRLB) is the most commonly used lower bound on time-delay variance [13]–[16]. The CRLB, however, can be achieved only for large post integration SNR [13],[14] and zero strain, conditions that are unrealistic for strain estimation. The expression of the CRLB derived by Walker and Trahey [17] (for partially correlated signals) increases the bound on the variance to a more achievable level. While electronic and quantization noise contributions (sonographic SNR, denoted by SNR_S) are accounted for in the expression for the CRLB through the SNR term [13]–[16], the added effect of decorrelation on the variance of the time delay estimate has been modeled recently by Walker and Trahey [17]. The authors also indicate that TDE performance can be worse than the CRLB at poor SNRs ($<$15 dB) and low correlation coefficient values ($<$0.5).

Signal decorrelation, a significant source of error in the displacement estimate, increases rapidly with tissue compression. Decorrelation errors are caused by the relative displacement of the scatterers in all three dimensions due to tissue compression. In this paper, signal decorrelation is modeled as a noise process that reduces the composite signal-to-noise ratio (SNR_C) in the echo-signal. SNR_C is a combination of the constant electronic noise level and a varying component due to signal decorrelation. To incorporate the contributions due to signal decorrelation it is necessary to convert the correlation coefficient to an SNR measure (SNR_ρ). A relationship between SNR_ρ and the correlation coefficient has been independently derived by Friemel [18], and by Céspedes *et al.* [12]. The expression used to obtain SNR_C is presented in Appendix A.

Increasing signal decorrelation errors with tissue strain reduce SNR_C, causing the strain estimation variance to exceed the CRLB (as also noted by Walker and Trahey [17]), thereby necessitating the need for a more advanced lower bound to predict the variance of the strain estimator. The modified Ziv-Zakai lower bound proposed by Weinstein and Weiss [13],[14] is used in this paper to obtain an accurate lower bound.

B. The Ziv-Zakai Lower Bound (ZZLB) on Time-Delay Estimation

Weinstein and Weiss present plots of the lower bound of the time delay variance versus the post integration SNR [13],[14] (defined as a product of the bandwidth, data window length, and the SNR_C), that divides the post integration SNR domain into three distinct regions (low, moderate, and high). Since SNR_C is the only parameter in the expression for the post integration SNR that varies with tissue strain, its value determines the appropriate lower bound.

The Cramér-Rao lower bound (CRLB) is applicable only to high post integration SNR situations (at low strains). In this region, time-delay estimation is subject only to local errors (ambiguity-free mode of operation). At moderate SNR values, the lower bound exceeds the CRLB and obeys the Barankin bound. In this region, ambiguities in the signal phase cannot be resolved; however, an estimate of the time-delay estimate may still be obtained using the correlation between signal envelopes. At low post integration SNR values, the lower bound approaches a constant level. In this region, both envelope and phase ambiguities exist, and the time delay cannot be estimated correctly. The thresholds separating these three regions are determined by the value of the post integration SNR [13],[14]. The above combination of lower bounds on the variance of the time-delay estimator is referred to as the Ziv-Zakai lower bound [13],[14]. The ZZLB provides the tightest bound on the variance of the time-delay estimator. The modified ZZLB and threshold values at the transition points are discussed in Appendix B.

In this paper, the strain variance is computed from the TDE variance using the expression derived by Walker and Trahey [17], as long as the ZZLB coincides with the CRLB. The decay in the value of the correlation coefficient with tissue compression has been modeled using an analytic expression derived by Meunier and Bertrand in [19] to estimate decorrelation effects due to rotation, translation, and biaxial deformation of the elastic tissue elements. The theoretical development of the strain filter is presented in the next section.

III. Development of the Strain Filter

Axial strain s is the displacement gradient, which may be estimated from two adjacent time delay estimates separated by a time interval Δt [1], assuming a constant speed of sound in the tissue, *viz*:

$$s = \frac{\tau_2 - \tau_1}{\Delta t} \quad , \tag{1}$$

where τ_1 is the time delay estimate at time t, and τ_2 is the time delay estimate at time $t + \Delta t$ for a data window with duration T.

Since the strain estimate is obtained from a linear combination of two random variables (time delay estimates separated by Δt), the variance of the strain estimator depends on the variance of the time delay estimator. Assuming stationarity, the variance of the strain estimate (σ_S^2) is expressed in terms of the variance of the time delay estimates (σ_t^2) in [20], and is given by:

$$\sigma_S^2 \geq \frac{2\sigma_\tau^2}{T\Delta t} \quad . \tag{2}$$

(2) illustrates that for a given window size and overlap, strain variance is reduced when the variance in the time delay estimate is minimized. The resolution in the elastogram is reduced with an increase in T. Large overlapping windows also generate correlated errors which bias the strain estimate. In addition, an optimal window size exists, where the strain estimation variance is minimum, with an increase in the variance observed as the window size is increased or decreased [6, pp. 122, 21]. Therefore the strain estimation variance cannot simply be reduced in the limit as $T \to \infty$, since σ_τ^2 also increases.

A. The Strain Filter in Elastography

A measure of elastographic image quality was described [6],[7] in terms of the mean to standard deviation ratio (SNR_e) of the elastogram:

$$SNR_e = \frac{\mu_s}{\sigma_s} \quad , \tag{3}$$

where μ_s and σ_s are, respectively, the mean and standard deviation of the strain estimates in a region of uniform elasticity. The upper bound of the SNR_e is obtained when the total tissue strain (s_t) and the lower bound on the strain estimation standard deviation (σ_{ZZLB}) are substituted in (3):

$$SNR_e^{UB} = \frac{s_t}{\sigma_{ZZLB}} \quad . \tag{4}$$

Incorporating the modified ZZLB expression for the TDE variance (see Appendix B) into σ_{ZZLB} using (2), we obtain:

$$\sigma_{ZZLB}^2 \geq \begin{cases} \frac{(sT)^2}{6T\Delta t}, & BTSNR_C < \gamma' \\ Threshold & \gamma' < BTSNR_C < \delta' \\ \frac{2\sigma_{BB}^2}{T\Delta t}, & \delta' < BTSNR_C < \mu' \\ Threshold & \mu' < BTSNR_C < \eta' \\ \frac{2\sigma_{CRLB}^2}{T\Delta t}, & \eta' < BTSNR_C \end{cases} \tag{5}$$

where η', μ', δ', and γ' are the modified thresholds (B-2) scaled by the factor $\frac{2}{T\Delta t}$. (5) shows the three distinct operating regions for σ_{ZZLB}^2, depending on the value of $BTSNR_C$. A distinct threshold region is observed between the CRLB and the Barankin bound; however, the variance increases exponentially in this threshold region (see Appendix B). Accurate estimation of the strain is possible only within the CRLB.

The minimum variance of the time delay estimator is given by the CRLB [13]–[17]. The CRLB for time delay estimation has been adapted for partially correlated signals by Walker and Trahey in [17], and is given by:

$$\sigma_{CRLB}^2 \cong \frac{3}{2\pi^2 T(B^3 + 12Bf_o^2)} \left[\frac{1}{\rho^2}(1 + \frac{1}{SNR^2})^2 - 1\right] \tag{6}$$

where f_o is the center frequency, B is the bandwidth, ρ is the correlation coefficient, and the SNR term represents only the contribution due to electronic noise (SNR_S). This closed-form expression obtained for signals with a rectangular spectrum assumes that the variance of the time delay estimate is bounded by the CRLB. The Barankin bound exceeds the CRLB by a factor of $12\left(\frac{f_0}{B}\right)^2$ [13],[14], and is given by:

$$\sigma_{BB}^2 = 12\left(\frac{f_o}{B}\right)^2 \sigma_{CRLB}^2 \tag{7}$$

The lower bound on the variance of the strain estimate (σ_{ZZLB}^2) is obtained by substituting the bound on the variance of the TDE obtained using (6) and (7) into (5).

The variation of SNR_e^{UB} (4) with tissue strain is defined as the strain filter. Three distinct regions constitute the strain filter, which depends on the appropriate lower bound that contributes to σ_{ZZLB}^2 (5).

B. Effect of Decorrelation Due to Strain on the Correlation Coefficient

Decorrelation errors increase with tissue strain, causing a decay in the values of the correlation coefficient. The correlation coefficient with motion compensation due to axial deformation of elastic tissue for a 2-D Gaussian model

has been derived by Meunier and Bertrand in [19], and is given by:

$$\rho = \frac{2\sqrt{\alpha\beta}}{\sqrt{2(\alpha^2+1)(\beta^2+1)}} e^{-\frac{1}{2}\left(\frac{f}{\sigma_u}\right)^2 \frac{(\alpha-1)^2}{\alpha^2+1}} \tag{8}$$

where f is the spatial frequency in cycles/mm ($f = \frac{2f_o}{c}$ where c is the speed of sound in tissue = 1.54 mm/s), and σ_f is the standard deviation of the Gaussian envelope in cycles/mm ($\sigma_u = \frac{2\sigma_f}{c}$, and $\sigma_f = \frac{1}{2\pi\sigma_t}$, where σ_t is the spatial standard deviation and σ_f is the standard deviation of the Gaussian envelope in the frequency domain), α represents the axial compression where $\alpha = 1 - s$, and s is the tissue strain. The corresponding lateral expansion is denoted by β (with the incompressibility constraint $\alpha\beta = 1$). The value of the correlation coefficient is substituted in the expression for the CRLB (6) to model decorrelation effects.

Expressions for the CRLB [13]–[17] have been derived for flat bandlimited signal and noise spectra. However, the correlation coefficient in [19] is derived for a Gaussian-shaped spectrum rather than a rectangular spectrum. A reasonable approximation was obtained by Céspedes *et al.* [11] using a rectangular spectrum centered at the Gaussian center frequency with the same mean square amplitude value as the Gaussian spectrum. The equivalent noise spectral bandwidth [22, pp. 141] is defined by:

$$B = \frac{\int_0^\infty P(f)\, df}{P(f)\,|_{\max}} = \sqrt{2\pi}\sigma_f \tag{9}$$

where B is the bandwidth of a rectangular spectrum with the same total power and peak amplitude as the Gaussian pulse spectrum $P(f)$.

Using the following typical signal parameters, T = 1 mm (1.3 μs), f_o = 5 MHz, B = 3 MHz (60% bandwidth), SNR_S = 100 (40 dB), and interval between strain estimates Δz = 0.5 mm (Δt = 0.66 μs). The lower bound on the standard deviation of the strain estimator (normalized by its value at 8% strain) is plotted along with the corresponding correlation coefficient in Fig. 2, for increasing strain values. Note from Fig. 2 that the lower bound on the standard deviation (σ_{ZZLB}) increases dramatically for strain values >0.5%. This has been previously noted by O'Donnell *et al.* [5] and Céspedes [6, pp. 115]. They show that the standard deviation of the strain for a 1-D simulation increases dramatically due to decorrelation associated with large strain values (>3%) for a fixed correlation integration time. For the same reason, past work in elastography has used small ($\leq$ 2%) applied strains [1],[2].

Decorrelation errors increase with tissue strain, reducing the value of the correlation coefficient, and causing σ^2_{ZZLB} to move from the CRLB to the Barankin bound or the constant variance level as shown in (5). The three distinct regions in (5) are observed in plots of the strain filter as shown by the curves in Fig. 3. Figure 3 shows the strain filter obtained for a 3 MHz rectangular bandwidth using the ZZLB (CRLB for strains $\leq$10%, Barankin bound for strains >10% and <30%, and the constant variance level for strains >30%). As the lower bound coincides

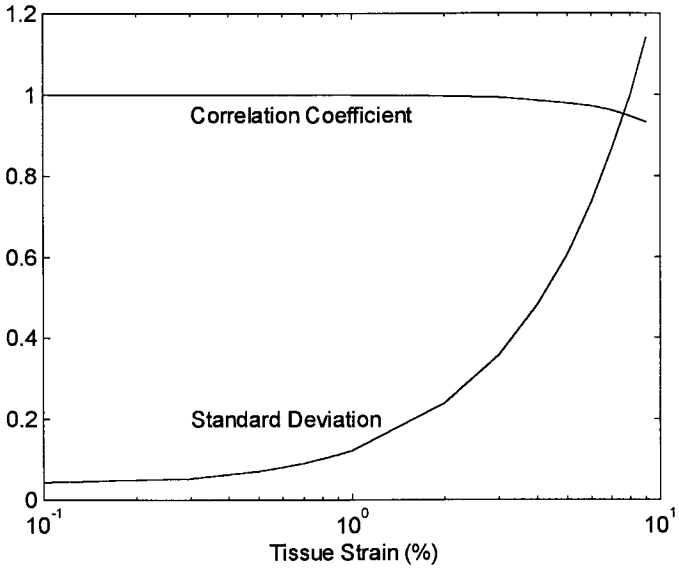

Fig. 2. The correlation coefficient and the standard deviation of the strain estimate for increasing strain values. The standard deviation of the strain estimate has been normalized by the standard deviation value at 8% strain of 0.0058 μs to enable plotting both the standard deviation of the strain estimate and the correlation coefficient on the same graph.

with the Barankin bound, the performance of the strain filter drops sharply, with a further drop in performance observed as the variance coincides with the constant variance level. Note that the strain filter obtained using the ZZLB has a smaller dynamic range than the strain filter obtained under the optimistic assumption that the strain estimation variance is always bounded by the CRLB.

The range of strains that can be reliably estimated using the elastogram determines the dynamic range of the strain filter. The dynamic range of the strain estimator in decibels is defined as follows:

$$DR = 20\log\left[\frac{s_{\max}}{s_{\min}}\right] \quad , \tag{10}$$

where $s_{\max}$ is the maximum strain and $s_{\min}$ is the minimum strain at a specified SNR_e level in the strain filter. The quantity $s_{\min}$ also defines the sensitivity of the strain filter. A 1% tissue strain corresponds to a decibel value of -40 dB. The dynamic range estimated for a -3 dB cutoff level of the strain filter (SNR_e level of 10) predicts a 30 dB dynamic range (observed from Fig. 3) for the strain filter obtained using the ZZLB bound, compared to the 40 dB dynamic range predicted using the CRLB. However, the dynamic range obtained experimentally for a single compression agrees closely with the dynamic range predicted using the ZZLB.

The slope of the strain filter for low strain values is determined primarily by electronic noise contributions, with decorrelation noise contributing to the progressive flattening of the curve. The plateau in the strain filter is caused by increasing decorrelation errors; however, the variance of the strain estimate is still bounded by the CRLB in this region. At high strain values, the precipitous drop in

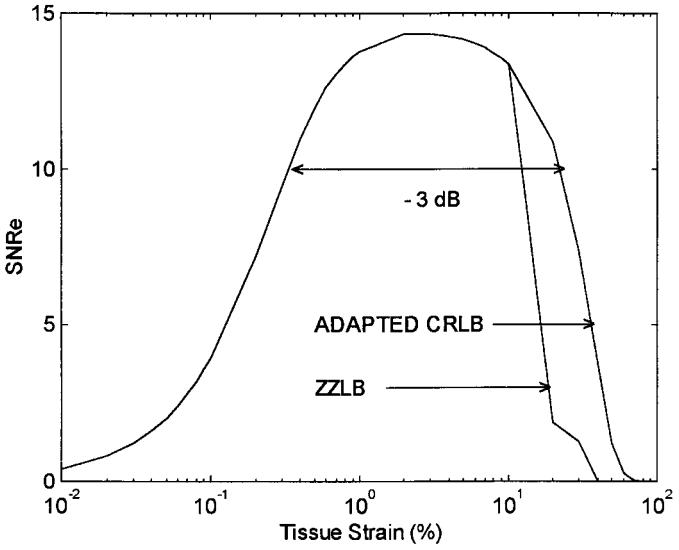

Fig. 3. The strain filter illustrating the distinct regions of strain estimation obtained using (5), along with the strain filter obtained under the optimistic assumption that the strain estimation variance is always bounded by the CRLB adapted for partially correlated signals. Note that the dynamic range of elastography may be determined from the width of the strain filter, and the heights give the respective SNR_e at every strain level.

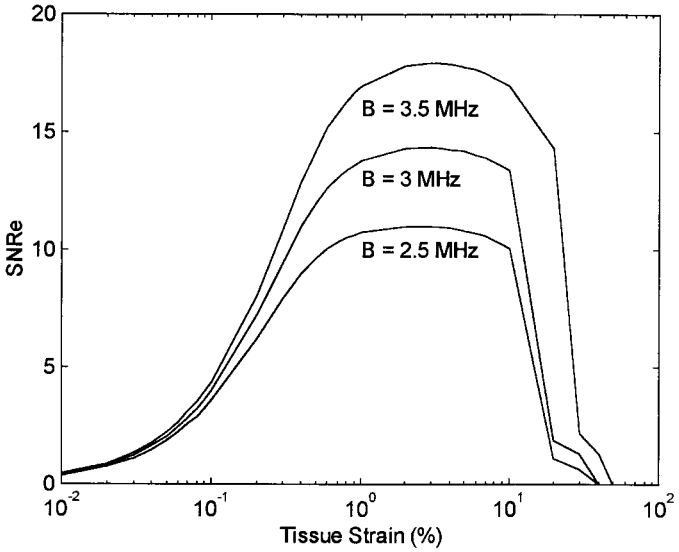

Fig. 4. A group of three strain filters, showing the distinct regions of strain estimation. These filters correspond to bandwidths of 2.5 MHz, 3 MHz, and 3.5 MHz, respectively, with a 5 MHz center frequency and $T = 1.3$ μs. Note the improvement in SNR_e and dynamic range obtained with an increase in the signal bandwidth.

performance is caused by decorrelation noise, which determines the slope of the graph in this region. Improvements in the dynamic range can be obtained either by reducing electronic noise errors for low values of the strain, or reducing the rate of decorrelation for large strain values. Decorrelation errors can be reduced using a combination of small compressions that allow successful step-wise temporal stretching. For example, temporal stretching of the post-compression signal [6]–[8], MA [5],[9], and [10], and SMA [9],[10] improves the dynamic range and SNR_e of strain estimation without sacrificing resolution.

The shape of the strain filter also depends on the variation of T, f_0, and B terms in the denominator of (6). For example, the performance of the strain filter for different values of the bandwidth is shown in Fig. 4. With an increase in the system bandwidth, there is an improvement in the maximum SNR_e value, sensitivity, and dynamic range of the strain filter. In other words, signal decorrelation reduces with an increase in the bandwidth. The strain filters obtained at different center frequencies are presented in Fig. 5. Note the improvement in the sensitivity, dynamic range, and SNR_e obtained with increasing pulse center frequency. The maximum attainable SNR_e is approximately proportional to the square of the center frequency.

The resolution of elastography depends on T and Δt, and is limited only by the correlation length of the ultrasound system. The resolution in the elastogram improves with a decrease in the value of T or an increase in system bandwidth. All the performance plots of the strain filter are plotted for a constant value of the resolution. A family of performance curves can be obtained at different resolution levels. In general, as resolution increases, the maximum value of the SNR_e and the dynamic range of the strain filter decrease. The dynamic range, sensitivity, and SNR_e, along with the resolution, provide a complete characterization of the noise properties in the performance of the strain estimator in elastography.

Simulation experiments in the next section are used to confirm the validity of the theoretical strain filter model developed in this section.

IV. Simulation

A simulation experiment to quantify the performance of the strain estimator for a 1-D tissue mechanical model is presented in this section. The 1-D model used in the simulation accounts only for the decorrelation of the echo-signal due to the axial component of the strain. The theoretical model can be adapted for the 1-D case by setting $\beta = 1$ in (8). In the simulation of the ultrasound system, a 1-D sampled array is used to insonify a 2-D point scatterer medium.

A. Method

The pre- and post-compression echo-signals are generated using a transducer with a center frequency of 5 MHz and -3 dB band-width of 3 MHz (pulse standard deviation of 0.27 μs). The A-scan was sampled at 50 MHz. Cross-correlation analysis was performed using a 1 mm (1.3 μs) overlapping window with 0.5 mm (0.66 μs) overlap between consecutive windows.

The transducer is modeled as a 1-D sampled aperture composed of point subtransducer elements equally spaced

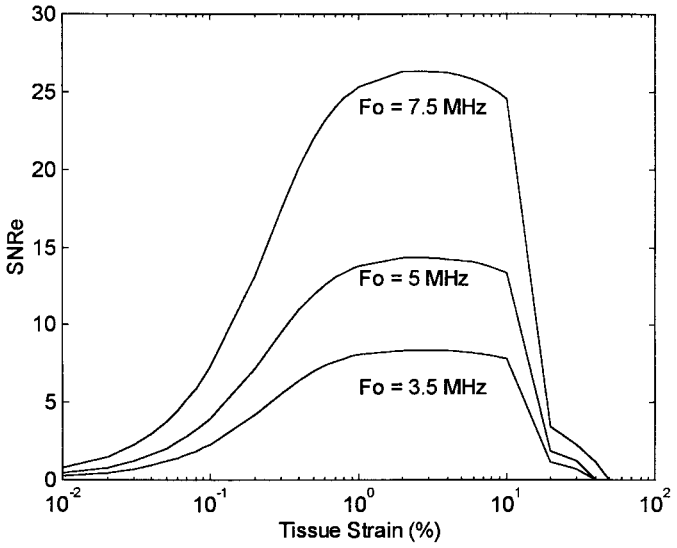

Fig. 5. A group of strain filters for center frequencies of 3.5 MHz, 5 MHz, and 7.5 MHz, respectively, with a 60% bandwidth and $T = 1.3\ \mu$s. Note the improvement in SNR_e and dynamic range obtained with an increase in the pulse center frequency. The maximum attainable SNR_e is approximately proportional to the square of the center frequency.

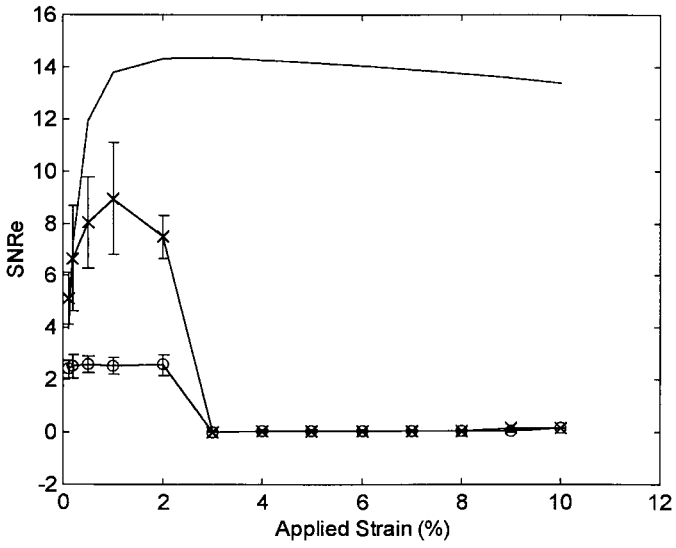

Fig. 6. Plot of the theoretical strain filter superimposed on the strain filters obtained using a 1-D simulation before (o o o) and after (x x x) temporal stretching (motion compensation).

by $\lambda/2$. Each subtransducer element is modeled as a point source or receiver with a two-way Gaussian transfer function. The scattering medium is modeled as a 2-D array of point scatterers. The scatterer density in the media was set to 48 scatterers/pulse width. The elastic target is assumed to have a Poisson's ratio ≈ 0. This implies that lateral and elevational decorrelation effects due to scatterer motion are ignored. The applied stress is assumed to propagate uniformly so the localized stress is constant throughout the medium. The displacement of each scatterer is a function of the applied strain, and is modeled by considering an equivalent 1-D spring system described in [6]. The spring constant is a function of the Young's modulus of the tissue. The applied strain is the same as the tissue strain for a uniformly elastic homogenous medium.

The pre-compression A-line is obtained from the randomly distributed scatterers. Each scatterer location is then changed depending on the compressive force and a post-compression A-line generated. The stretched post-compression A-line is generated by applying a linear stretch factor on the post-compression signal. The process is repeated for 28 different lateral locations in the simulated phantom to obtain independent A-line pairs (lateral step > beamwidth of the transducer). The strain values are computed from the individual A-line pairs. Time-delay estimation is performed using the normalized cross-correlation function, with the strains computed using (1).

B. Results

Fig. 6 shows the mean SNR_e value and its standard deviation (error bars), derived from 28 independent simulations, before and after temporal stretching. The x-axis represents the total applied compressive strain expressed as a percentage; SNR_e is plotted, along the y-axis. The theoretical curve of the strain filter for the 1-D case is also shown in the figure.

Observe from Fig. 6 that both the strain filter curves obtained from the simulation are completely bounded by the theoretical strain filter curve. The theoretical strain filter curve forms the upper bound, which determines the attainable experimental or simulation performance. For strain values >2%, decorrelation errors cause the drop in the value of the estimated strain. The CRLB bound on the variance is no longer applicable for strain values >2%, as shown by the simulation experiment, since signal decorrelation introduced due to tissue compression dramatically increases the variance in the strain estimate.

Inaccurate estimation of the time-delay (increased variance) is primarily due to the detection of false peaks and jitter [17]. The simulation results presented in this section are obtained using the basic normalized correlation coefficient function. Non-linear processing to remove phase ambiguities (contributing to the reduction of false peaks [17]) was not performed. Sophisticated algorithms that incorporate additional processing to remove false peaks can therefore significantly improve the performance of the strain estimator.

V. Conclusion

This paper presents a theoretical framework for quantitative assessment of the quality of elastograms. This framework is described as a strain filter that is typically a band-pass filter in the strain domain. This filter allows only a restricted range of strain values to be included in the elastogram. The deviation of the strain filter from an ideal all-pass characteristic in the strain domain is due to the ultrasound system parameters, the finite value of the sono-

graphic SNR, and the effects of signal decorrelation. Signal decorrelation determines the largest value of strain that is accurately estimated, while SNR_S determines the smallest measurable strain value. The dynamic range of the system is thus limited on the low end by electronic noise effects, and on the high end by signal decorrelation, resulting in a bandpass filter in the strain domain.

The range of strains over which the CRLB specifies the variance of the time delay defines the optimum performance range for the strain estimator. The formulation of the CRLB by Walker and Trahey does not address the implications of decorrelation causing the deviation of the time delay variance from the CRLB for large tissue strains. Application of the $\rho - SNR_\rho$ relationship developed by Friemel [18] and Céspedes *et al.* [12] clearly demarcates the regions over which the CRLB, the Barankin bound, and the constant variance level are applicable. Signal decorrelation may be reduced using a combination of small compressions that allow successful temporal stretching, (e.g., temporal stretching described by Céspedes and Ophir [6]–[8], and SMA described by Huang *et al.* [9],[10]). Temporal stretching is currently used to correct for decorrelation only along the axial direction. Lateral and elevational decorrelation errors are more difficult to correct, since the scatterers move out of the beam for large strains. Multicompression averaging in conjunction with temporal stretching of the strain estimates obtained from several small compressions, increases both the SNR_e and the dynamic range of strain estimation without sacrificing resolution. The improvements in the elastogram obtained using these techniques may be quantitatively predicted using the theoretical strain filter model developed in this paper.

The strain filter concept developed in this paper provides a graphical framework for characterizing elastography. The strain filter quantified the elastogram image quality (−3 dB dynamic range 30 dB using the ZZLB and maximum elastogram $SNR_e \approx 23$ dB for a single compression), for the signal parameters specified in Section III. In a similar manner, different elastographic signal processing techniques can now be compared and their performance quantified using the dynamic range, sensitivity, resolution, and maximum SNR_e obtained from the strain filter. The shape of the strain filter defines the quality of the elastogram; a narrow, low filter will cause elastographic artifacts such as image noise and low dynamic range to plague the elastogram. Thus, the design of the optimal strain filter for a given situation is of utmost importance to the production of quality elastograms.

The signal decorrelation parameter and shape of the strain filter vary with changes in the cross-correlation window length (resolution) used to obtain the time-delay. A family of strain filter curves can be obtained at different resolution levels. The effect of the window length parameter on signal decorrelation has not been analyzed in this paper. The dependence of the correlation coefficient on the finite window length used in the cross-correlation analysis is discussed in [21]. The expression for the effective correlation coefficient is presented as a product of the peak value of the correlation coefficient (used in this paper) and a derating factor. The derating factor accounts for the decay in the correlation coefficient with increased window lengths. The strain filter described in this paper is therefore more optimistic in its prediction of the strain estimator performance. In addition, the strain filters obtained at varying depths in tissue also would be different. The 2-D and nonstationary properties of the strain filter will be discussed in a later publication. It has also been demonstrated that under certain conditions, i.e. optimal multicompression with temporal stretching [23], the bandpass characteristic of the strain filter changes into a more desirable, high-emphasis characteristic.

Acknowledgments

The authors would like to thank Dr. Ignacio Céspedes for the many discussions, and Dr. Michel Bertrand and Dr. S. Kaiser Alam for their helpful comments.

Appendix A

A. Combining SNR_S and SNR_ρ to obtain SNR_C

The expression for SNR_C which is used to compute the post integration SNR and the thresholds in the ZZLB is presented here. The correlation coefficient is converted into an SNR measure [7],[18], that is given by:

$$SNR_\rho = \frac{\rho}{1-\rho} \quad . \tag{A.1}$$

The variation of SNR_ρ with a linear variation in ρ is illustrated in Fig. 7. Note from (A-1) that for $\rho = 1$, $SNR_\rho = \infty$, dropping exponentially to an SNR_ρ value of 22.46 dB for $\rho = 0.93$. The composite value of the SNR, combining the contributions of SNR_S and SNR_ρ is given by [13],[14]:

$$SNR_C = \frac{SNR_S SNR_\rho}{1 + SNR_S + SNR_\rho} \quad . \tag{A.2}$$

This expression for SNR_C incorporates both the electronic noise level and the decrease in SNR caused by increase in signal decorrelation with strain. From (A.2) we observe that SNR_C will always be bounded by the smallest value of either SNR_S or SNR_ρ.

Appendix B

B. Lower Bound on the Variance of the Time Delay Estimator

The modified ZZLB derived by Weinstein and Weiss [13],[14] gives the tightest lower bound on the TDE variance. We present here the results for bandpass signals with

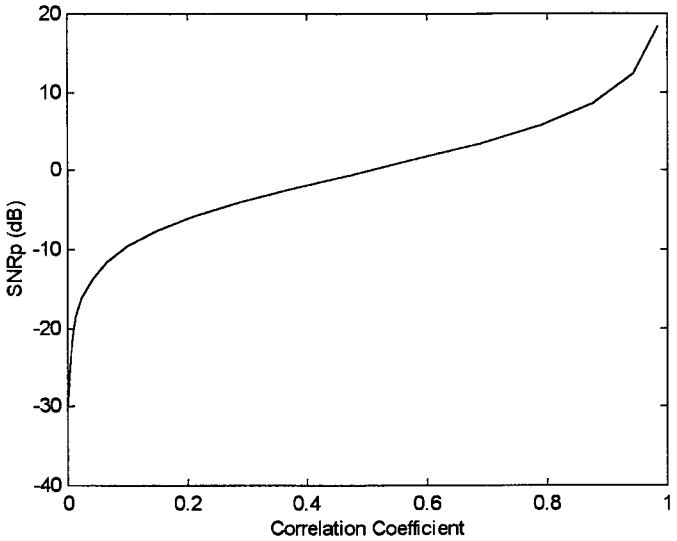

Fig. 7. Plot of the non-linear variation of SNR_ρ with the correlation coefficient.

a rectangular spectrum. The lower bound for the time delay estimation consists of two distinct threshold effects dividing the entire post integration SNR domain into three disjointed segments (the CRLB, Barankin bound, and the constant variance level), as shown by Fig. 7 and (22) in [14]. The distinct regions using (22) from [14] are given by:

$$\sigma_\tau^2 \geq \begin{cases} (sT)^2/12, & BTSNR_C < \gamma \\ Threshold, & \gamma < BTSNR_C < \delta \\ \sigma_{BB}^2, & \delta < BTSNR_C < \mu \\ Threshold, & \mu < BTSNR_C < \eta \\ \sigma_{CRLB}^2, & \eta < BTSNR_C \ , \end{cases} \tag{B.1}$$

where the estimate of the time delay is confined to the interval $-sT/2 < \tau < sT/2$, T is the length of the cross-correlation window, B is the bandwidth of the system, σ_{BB}^2 represents the Barankin bound, and σ_{CRLB}^2 represents the CRLB. The quantity $BTSNR_c$ is referred to as the post integration SNR. The threshold points used in (B-1) are defined as follows:

$$\begin{aligned} \eta &= \frac{6}{\pi^2}\left(\frac{f_0}{B}\right)^2\left[\varphi^{-1}\left(\frac{B^2}{24f_0^2}\right)\right]^2 \\ \mu &= \frac{2.76}{\pi^2}\left(\frac{f_o}{B}\right)^2 \\ \delta &= \zeta/2 \\ \gamma &\approx 0.46 \ , \end{aligned} \tag{B.2}$$

where f_o is the center frequency, $\varphi^{-1}(y)$ is the inverse of $\varphi(y) = \frac{1}{\sqrt{2\pi}}\int_y^\infty e^{-\mu^2/2}d\mu$, and $(\zeta/2)\varphi(\sqrt{\zeta/2}) = (12\pi/BsT)^2$, which has two solutions. The larger value of ζ is used to compute the threshold.

When $\eta < BTSNR_c$, the ZZLB coincides with the CRLB, which is the ambiguity-free region. If $\delta < BTSNR_c < \mu$, the ZZLB coincides with the Barankin bound, where phase ambiguities increase the TDE variance. Finally, when $BTSNR_c < \gamma$, the lower bound is characterized by the constant variance level of $(\epsilon T)^2/12$, which corresponds to the variance of a random variable uniformly distributed between $-sT/2 < \tau < sT/2$. In the threshold region, the TDE variance increases exponentially with the post integration SNR.

The thresholds given in (B.2) are computed for the following typical signal parameters: $T = 1$ mm (1.3 μs), $f_o = 5$ MHz, $B = 3$ MHz (60% bandwidth), and $SNR_S = 40$ dB. Assuming $SNR_\rho \gg 40$ dB, $SNR_C \approx 40$ dB. The numerical values of the thresholds η, μ, δ, and γ and in (B-2) are 13.52, 0.78, 0.59, and 0.46 (22.6, -1.1, -2.3, and -3.4 when expressed in dB), respectively, at a post integration SNR value of 43.86 dB. The reader is referred to the papers by Weinstein and Weiss [13],[14] for a detailed description and derivation of the ZZLB and the thresholds for narrow and wide-band systems.

References

[1] J. Ophir, E. I. Céspedes, H. Ponnekanti, Y. Yazdi, and X. Li, "Elastography: a quantitative method for imaging the elasticity of biological tissues," *Ultrason. Imag.*, vol. 13, pp. 111–134, 1991.

[2] E. I. Céspedes, J. Ophir, H. Ponnekanti, N. Maklad, "Elastography: Elasticity imaging using ultrasound with application to muscle and breast *in vivo*, *Ultrason. Imag.*, vol. 15, (2), pp. 73–88, 1993.

[3] M. Bertrand, M. Meunier, M. Doucet, and G. Ferland, "Ultrasonic biomechanical strain gauge based on speckle tracking," *Proc. 1989 IEEE Ultrason. Symp.*, pp. 859–864.

[4] H. E. Talhami, L. S. Wilson, and M. L. Neale, "Spectral tissue strain: A new technique for imaging tissue strain using intravascular ultrasound," *Ultrasound, Med. Biol.*, vol. 20, no. 8, pp. 759–772, 1994.

[5] M. O'Donnell, A. R. Skovoroda, B. M. Shapo, and S. Y. Emelianov, "Internal displacement and strain imaging using ultrasonic speckle tracking," *IEEE Trans. Ultrason., Ferroelect., Freq. Contr.*, vol. 41, no. 3, pp. 314–325, 1994.

[6] E. I. Céspedes, "Elastography: Imaging of Biological Tissue Elasticity," *Ph.D. Dissertation*, University of Houston, 1993.

[7] E. I. Céspedes and J. Ophir, "Reduction of image noise in elastography," *Ultrason. Imag.*, vol. 15, pp. 89–102, 1993.

[8] M. Bilgen and M. F. Insana, "Deformation models and correlation analysis in elastography," *J. Acoust. Soc. Am.*, vol. 99, no. 5, pp. 3212–3224, 1996.

[9] Y. Huang, E. I. Céspedes, and J. Ophir, "Techniques for noise reduction in elastograms," Abstract, *AIUM*, 1995.

[10] T. Varghese, J. Ophir, and E. I. Céspedes, "Noise reduction in elastography using temporal stretching with multicompression averaging," *Ultrasound Med. Biol.*, vol. 22, no. 8 pp. 1043–1052, 1996.

[11] E. I. Céspedes, Y. Huang, J. Ophir, and S. Spratt, "Methods for estimation of subsample time delays of digitized echo signals," *Ultrason. Imag.*, vol. 17, pp. 142–171, 1995.

[12] E. I. Céspedes, J. Ophir, and S. K. Alam, "The combined effect of signal decorrelation and random noise on the variance of time delay estimation," *IEEE Trans. Ultrason., Ferroelect., Freq. Contr.*, vol. 44, no. 1, pp. 220–225, 1997.

[13] E. Weinstein and A. Weiss, "Fundamental limitations in passive time delay estimation- Part I: Narrow-band systems," *IEEE Trans. Acoust., Speech, Sig. Proc.*, vol. ASSP-31, no. 2, pp. 472–485, 1983.

[14] E. Weinstein and A. Weiss, "Fundamental limitations in passive time delay estimation- Part II: Wide-band systems," *IEEE Trans. Acoust., Speech, Sig. Proc.*, vol. ASSP-31 (5), pp. 1064–1078, 1984.

[15] A. H. Quazi, "An overview of the time delay estimate in active and passive systems for target localization," *IEEE Trans. Acoust., Speech, Sig. Proc.*, vol. ASSP-29, pp. 527–533, 1981.

[16] C. H. Knapp and G. C. Carter, "The Generalized correlation method for estimation of time delay," *IEEE Trans. Acoust., Speech, Sig. Proc.*, vol. ASSP-24, pp. 320–327, 1976.
[17] F. W. Walker and E. G. Trahey, "A fundamental limit on delay estimation using partially correlated speckle signals," *IEEE Trans. Ultrason., Ferroelect., Freq. Contr.*, vol. 42, pp. 301–308, 1995.
[18] B. H. Friemel, "Real-time ultrasonic two-dimensional vector velocity estimation utilizing speckle-tracking algorithms: Implementation and limitations," *Ph.D Dissertation*, Duke University, 1994.
[19] J. Meunier and M. Bertrand, "Ultrasonic texture motion analysis: theory and simulation," *IEEE Trans. Ultrason., Ferroelect., Freq. Contr.*, vol. 14, pp. 293–300, 1995.
[20] E. I. Céspedes, M. F. Insana, and J. Ophir, "Theoretical bounds on strain estimation in Elastography," *IEEE Trans. Ultrason., Ferroelect., Freq. Contr.*, vol. 42, no. 5, pp. 969–972, 1995.
[21] T. Varghese, M. Bilgen, J. Ophir, and M. F. Insana, "Multiresolution strain filter in elastography," Submitted to *IEEE Trans. Ultrason., Ferroelect., Freq. Contr.*, 1996.
[22] J. S. Bendat and A. C. Piersol, *Random Data: Analysis and Measurement*, 2nd ed., New York: John Wiley, 1986.
[23] T. Varghese and J. Ophir, "Performance optimization in elastography: Multicompression with temporal stretching," (in press), *Ultrason. Imag.*, 1996.

Tomy Varghese (S'92–M'95) received the B.E. degree in instrumentation technology from the University of Mysore, India, in 1988, and the M.S. and Ph.D. in electrical engineering from the University of Kentucky, Lexington, KY in 1992 and 1995, respectively. From 1988 to 1990 he was employed as an Engineer in Wipro Information Technology Ltd., India. He is currently a post-doctoral research associate at the Ultrasonics Laboratory, Department of Radiology, The University of Texas Medical School, Houston. His current research interests include detection and estimation theory, statistical pattern recognition, tissue characterization using ultrasound, and signal and image processing applications in medical imaging. Dr. Varghese is a member of the IEEE and Eta Kappa Nu.

Jonathan Ophir received his B.S.E.E. (summa cum laude), M.S.E.E., and Doctor of Engineering degrees from the University of Kansas, Lawrence Kansas in 1971, 1973, and 1977, respectively. His Doctoral dissertation describes an early implementation of digital scan conversion techniques for diagnostic ultrasound. During 1976–1977 he worked as a project engineer for Philips Ultrasound Inc., where he developed a commercial version of their first Digital Scan Converter. He then spent three years as an Assistant Professor of Radiology at the University of Kansas Medical School in Kansas City, where he was involved in the development of prototype sonographic contrast agents, ultrasound phantoms, and instrumentation for ultrasonic tissue characterization. From 1980 until the present time, he has been with the University of Texas Medical School at Houston, where he is currently Professor of Radiology. He is also Adjunct Professor of Electrical Engineering at the University of Houston. His current field of interest is elastography, the imaging of the elastic properties of soft tissues. Dr. Ophir has contributed more than 85 papers to peer-reviewed scientific journals, and holds 15 US and foreign patents. He is a Fellow of the American Institute of Ultrasound in Medicine, past Chairman of their standards committee, and past member of the board of governors. He is a member of the Editorial Board of Ultrasound in Medicine and Biology, and is Associate Editor of *Ultrasonic Imaging*. In 1992 he received the Terrance Matzuk Award from the American Institute of Ultrasound in Medicine, and in 1995 he was recognized as Inventor of the Year by the mayor of the city of Houston, Texas. In 1995 he also received an honorary commission as an Admiral in the Texas Navy by Governor George W. Bush.